



Cite this: *New J. Chem.*, 2014,
38, 6103

Strawberry-like $\text{SiO}_2@\text{Pd}$ and Pt nanomaterials†

Alfonso Cornejo,^{a,b} Gad Fuks,^a Víctor Martínez-Merino,^b Íñigo Sarobe,^b María José Gil,^b Karine Philippot,^{c,d} Bruno Chaudret,^a Fabien Delpech^{*a} and Céline Nayral^{*a}

Based on a synthesis strategy of silica nanoparticles (NPs) in non-alcoholic medium, a straightforward protocol leading to strawberry-like $\text{SiO}_2@\text{M}$ nanomaterials ($\text{M} = \text{Pt}, \text{Pd}$) has been developed. Pd and Pt NPs were immobilised onto surface modified silica NPs, by *in situ* decomposition of organometallic precursors, $\text{Pd}_2(\text{dba})_3$ and $\text{Pt}(\text{dba})_2$ ($\text{dba} = \text{dibenzylideneacetone}$). The surface of silica was functionalised by aminopropyltriethoxysilane (APTES) or 2-(diphenylphosphino)ethyltriethoxysilane (PhPETES). The co-grafting of propyltriethoxysilane (PTES) and APTES was investigated to avoid the classical interfering cohydrolysis and polycondensation reactions which can lead to agglomeration phenomena between the silica NPs. It appeared that a APTES/PTES ratio of 1/3 insured a dense and homogeneous deposition of the metallic NPs onto silica. Depending on the ligand, the diameter of the metallic NPs varies from 3.6 to 6.0 nm for Pd and from 1.5 to 3.1 nm for Pt NPs. The metal loading is adjustable, at least up to 6.91 wt%, as exemplified with Pd. Preliminary catalytic tests of the $\text{SiO}_2@\text{Pd}$ nanomaterial are also presented.

Received (in Montpellier, France)
20th June 2014,

Accepted 29th September 2014

DOI: 10.1039/c4nj01019a

www.rsc.org/njc

Introduction

After a first phase of ever-increasing interest for the synthesis of NPs exhibiting controlled size, shape and composition, the development of complex nanomaterials associating different NPs is today one of the main goals in nanoscience. The ability to selectively arrange nanosized domains of different materials into a single hybrid NP is a key to enlarge the potentialities of these objects in terms of multiple functionalities, of enhanced properties or of compatibility with applications. In this context, the synthesis of hybrid metal–silica nanomaterials appears strategic to take advantage of the stability, biocompatibility, accessibility and easy surface functionalization of silica, combined with the properties (electronic, magnetic, optical or catalytic) of the metallic NPs.¹

For example, well dispersed NPs in the liquid phase are very attractive in terms of catalytic performances due to their high surface/volume ratio. However, to satisfy the environmental requirements and work with simple protocols associating easy

recovery and recyclability (which are still challenging for homogeneous catalysis processes), the catalytic NPs often have to be supported.^{2–4} Typical supports consist of mesoporous materials for which diffusion is limited by the pores that can induce a decrease of the catalytic activity.⁵ This drawback has triggered the synthesis of soluble but isolable substrates such as magnetic or centrifugable particles^{2,3,6,7} that overcome diffusional limitations. If silica (embedding or not a magnetic core) appears as a good candidate to play the role of a support,⁸ the achievement of reproducible syntheses of supported metal NPs, showing well-defined composition, small diameters (<10 nm) and narrow size distribution, is not trivial. A first synthetic strategy consists of anchoring M^{n+} species on the silica surface and forming metal NPs in a further reductive step (*e.g.* for Pd,⁹ Ru,¹⁰ or Pt¹¹) or during a catalytic cycle (*e.g.* for Pd,^{5,12,13} or Rh^{14,15}). A second strategy, which offers a better control of synthesis, is based on the impregnation of silica NPs, functionalized by a thiol or an amine, with preformed metallic NPs. The functional groups present at the surface of the silica allow the covalent linking of the metal NPs during the impregnation step (exemplified by Halas *et al.* for the immobilization of Au NPs,¹⁶ or by Gude *et al.* in the case of Pd NPs¹⁷). A third approach is based on the formation of the metal NPs (Pt¹⁸ or Pd¹⁹) by a direct nucleation on the silica surface. For example, the decomposition of an organometallic complex of Pd led to the formation of Pd NPs at the silica surface which had been previously functionalized by amino or terpyridine groups.¹⁹

In all of these cases, the synthesis of the final nanomaterial was achieved by multi-step processes involving therefore tedious

^a Université de Toulouse, INSA, UPS, CNRS, LPCNO (Laboratoire de Physique et Chimie des Nano-Objets), 135 avenue de Rangueil, F-31077 Toulouse, France.
E-mail: fdelpach@insa-toulouse.fr, cnayral@insa-toulouse.fr

^b Dpto. de Química Aplicada, Ed. "Los Acebos", Campus de Arrosadia, Universidad Pública de Navarra, E31006, Pamplona, Spain

^c CNRS, LCC (Laboratoire de Chimie de Coordination du CNRS), 205 route de Narbonne, BP 44099, F-31077 Toulouse, France

^d Université de Toulouse, UPS, INPT, F-31077 Toulouse Cedex 4, France

† Electronic supplementary information (ESI) available. See DOI: 10.1039/c4nj01019a

separation and purification procedures. Silica NPs (or shells) are prepared using the classical water/alcohol media which is not directly compatible with organometallic chemistry. Herein, we present a novel straightforward protocol for the synthesis of a family of nanomaterials based on Pd or Pt NPs immobilized on silica NPs, thanks to the silica surface functionalization either by an amine ligand or a phosphine ligand. The originality of the approach is based on a same synthetic medium (non-alcoholic solvent) for the formation of the metallic NPs and of the silica NPs. Indeed, the silica NPs have been prepared according to an original method involving tetrahydrofuran or dimethoxyethane that we have previously described.²⁰ These conditions are perfectly compatible with the synthesis of metallic NPs by decomposition of organometallic precursors which has been developed by our group.^{21–26} In the present paper, Pd and Pt NPs have been immobilized on the silica surface by decomposition of $\text{Pd}_2(\text{dba})_3$ and $\text{Pt}(\text{dba})_2$ in THF, in the presence of the preformed silica NPs. This method allows a simplification of the protocol and the formation of a very homogeneous distribution of the metallic NPs at the surface of silica. Besides the characterization of the nanomaterials by state-of-the art techniques, preliminary catalytic tests are presented.

Results and discussion

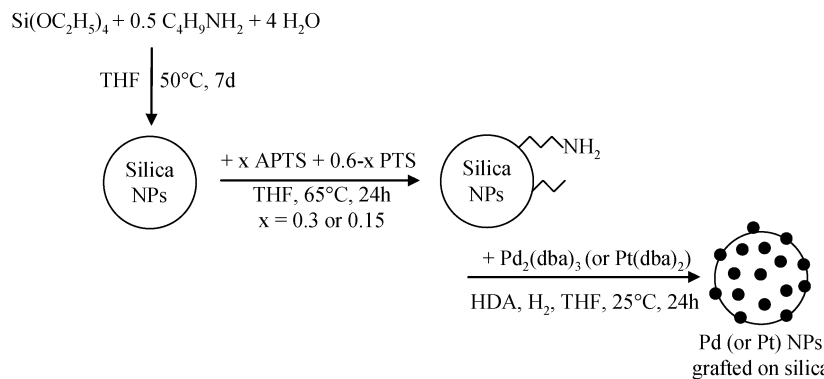
Strawberry-like nano-objects based on amine surface-modified silica NPs

We first examined the direct decomposition of $\text{Pd}_2(\text{dba})_3$ and $\text{Pt}(\text{dba})_2$ in THF, in the presence of the preformed silica NPs prepared according to the procedure previously described by our group (in a typical experiment the silica NPs exhibit a diameter centred at 88 ± 20 nm).²⁰ However, our attempts of grafting metallic NPs on unfunctionalized silica particles have been unsuccessful, leading to the formation of aggregated metallic NPs unlinked to silica, as previously observed by Guerrero *et al.*¹⁹ Therefore, the silica surface has been beforehand functionalized. In the first part of this work, the ligand chosen for surface modification is aminopropyltriethoxysilane (APTES). This is a bi-functional ligand frequently used to provide an amine function on the silica surface^{9,10,14,15,27} and which has shown to be an efficient stabilizer,

via the amine function, for metallic NPs (such as Ru).²⁸ However, it may induce agglomeration phenomena between the silica NPs, for which a few precedents exist in the literature and which are reasonably explained by cohydrolysis and polycondensation reactions, as the silica formation occurs by base-catalysed hydrolysis and condensation of TEOS.¹⁷ We indeed observed such a phenomenon, when adding APTES to the silica particles that coagulated then into larger objects. We could overcome this major drawback by grafting on the silica surface a mixture of APTES and propyltriethoxysilane (PTES) instead of solely APTES. Additionally, the addition of PTES also had a beneficial effect on the dispersion of the silica particles in apolar solvents.

The synthesis is carried out following a one-pot reaction involving three steps (Scheme 1). A solution of tetraethoxysilane (TEOS), butylamine (BA) and water with 1/0.5/4 molar ratios in THF is stirred at 50 °C for 7 days ($[\text{TEOS}] = 0.12\text{ M}$) to obtain a suspension of silica NPs. Then, a mixture of grafting ligands (APTES and PTES in different ratios, TEOS/(APTES + PTES) ratio of 1/0.6) is added to the raw suspension. Pd (or Pt) precursor and hexadecylamine (HDA, which improves the dispersion of the silica NPs in solution) are thereafter added into the reaction medium which is then pressurized under 3 bar of dihydrogen to provide the decomposition of the complex. No intermediate washing steps are required.

In the case of Pd, when an APTES/PTES ratio of 1/1 is used, agglomerates of Pd NPs are observed on the silica support (Fig. 1). High Resolution Transmission Electron Microscopy (HRTEM) together with the fast Fourier transform (FFT) pattern revealed lattice fringes separated by distances of 0.194 nm and 0.224 nm, corresponding, respectively, to the (200) and (111) lattice spacings of the face-centred cubic (fcc) palladium cell (Fig. 2). The grafting of this pair of ligands impacts the silica NPs size and morphology leading to larger silica nano-objects with a mean diameter of 207 ± 78 nm (Fig. 1, left). Due to the catalytic role of APTES and the absence of intermediate washing steps, further condensation reactions (involving triethoxysilyl species) and coalescence phenomena occur in solution. When the APTES/PTES ratio is decreased to 1/3, a homogeneous dispersion of Pd NPs (with a mean diameter of 3.6 (0.8) nm) on the silica surface is obtained (Fig. 1), with only a slight increase of the diameter and an enlargement of the size distribution of the silica NPs



Scheme 1 Synthesis of Pd NPs immobilized on amino-functionalized silica NPs.

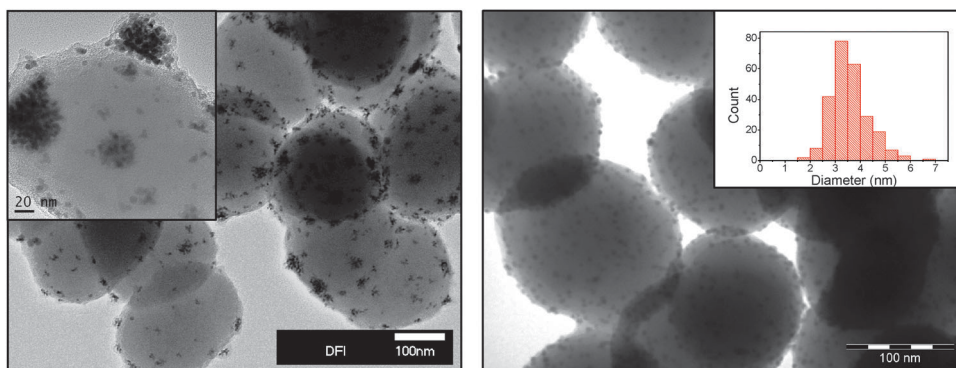


Fig. 1 TEM images of Pd NPs immobilised onto silica particles functionalized with APTES/PTES 1/1 (left) and APTES/PTES 1/3 (right with inserted size distribution).

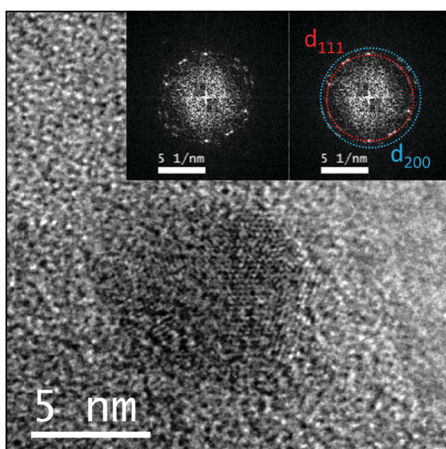


Fig. 2 HRTEM image of Pd NPs immobilised onto silica particles functionalized with APTES/PTES 1/1 and its FFT pattern (inset).

(APTES being in lower quantity). The $\text{SiO}_2@\text{Pd}$ nanomaterials are purified by centrifugation and washing with THF. Inductively-coupled plasma mass spectrometry (ICP-MS) shows that 65% of the introduced Pd has been immobilised onto silica and the Pd content on the support is then about 2.94 wt%. This Pd loading can be increased up to 6.91 wt% (Pd NPs keeping the same size and morphology) just by doubling the amount of Pd complex introduced (the Pd grafting yield is then about 52%). The versatility of this protocol enables us to vary and control the Pd weight contents of the nanomaterials.

These nanomaterials have been characterized by magic angle spinning (MAS) solid-state NMR which provided valuable information about the silica structure. It allows a direct comparison between the two samples (APTES/PTES = 1/1 or 1/3) and a rationalisation of the results. In both cases, the $^{29}\text{Si}\{^1\text{H}\}$ NMR spectrum (Fig. S1 and S2, ESI[†]) displays the Q substructure silicon signals (*i.e.*, corresponding to silicon atoms forming four Si–O bonds) and T substructure silicon signals (*i.e.*, corresponding to silicon atoms forming three Si–O bonds and one Si–C) which, respectively, belong to the inorganic core of the silica NPs and, to APTES and PTES grafted on the surface. The proportions of the Q (Q_2 : $\text{Si}(\text{OSi})_2(\text{OR})_2$, -91 ppm; Q_3 : $\text{Si}(\text{OSi})_3\text{OR}$, -101 ppm; Q_4 : $\text{Si}(\text{OSi})_4$, -110 ppm with R = H,

Et, or negative charge) and the T species (T_2 : $\text{C-Si}(\text{OSi})_2(\text{OR})$, -60 ppm; T_3 : $\text{C-Si}(\text{OSi})_3$, -68 ppm) are obtained from deconvolution of the $^{29}\text{Si}\{^1\text{H}\}$ spectrum. Two main pieces of information can be extracted from the analysis of these NMR data. First, the spectra are very similar except that in the case of the APTES/PTES ratio equal to 1/1, no T_2 or Q_2 are detected, indicating a higher degree of condensation. This observation is consistent with the presence in the reaction mixture of higher amounts of amine function which catalyzes a further condensation reaction of the alkoxy silyl moiety. Second, the relative percentage of all T (12%) and of all Q (88%) substructure species remains constant indicating that the sum of the amounts of APTES and PTES that are grafted on the NPs is the same. In other words, the degree of functionalization of the silica NPs is constant whatever the introduced APTES/PTES ratio, suggesting an optimal coverage of the silica surface. The conditions to obtain a regular distribution of organic units on the surface of bifunctional silica materials are difficult to predict,²⁹ but in the case of the 1/3 APTES/PTES ratio, the amine functions are presumably more homogeneously distributed over the silica surface, thus leading to a homogeneous dispersion of Pd NPs as mentioned before.

Similarly, Pt NPs of a mean diameter of 1.5 (0.3) nm, and homogeneously dispersed onto the silica surface, are formed by decomposition of $\text{Pt}(\text{dba})_2$ under 3 bar of dihydrogen at room temperature (Fig. 3). ICP-MS analysis revealed a Pt grafting yield which is *ca.* 56% and a Pt content in the nanomaterial of 2.14 wt%. The HRTEM image together with the FFT pattern showed lattice fringes separated by distances of 0.226 nm and 0.196 nm, corresponding, respectively, to the (111) and (200) lattice spacings of the fcc platinum (Fig. 4).

Strawberry-like nano-objects based on phosphine surface-modified silica NPs

In a second part of this work, we modified the interaction between the grafted ligand and the metallic NPs, by replacing the amino function by a phosphine one. Indeed, the phosphine function is expected to be a stronger coordinating ligand, as previously shown upon the stabilization of Pd or Pt NPs.^{30,31} The silica NPs have been thus functionalised by 2-(diphenylphosphino)ethyltriethoxysilane

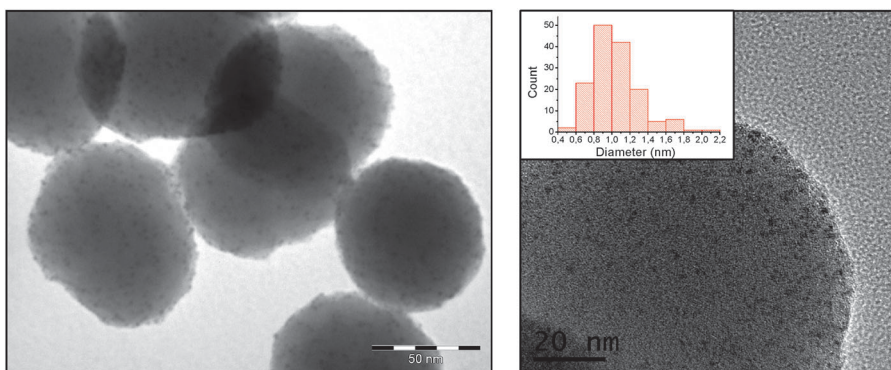


Fig. 3 TEM image (left) and HRTEM image (right with inserted size distribution) of Pt NPs immobilised onto silica NPs functionalized with APTES/PTES 1/3.

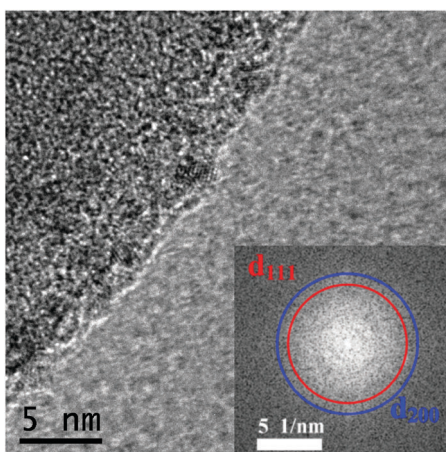
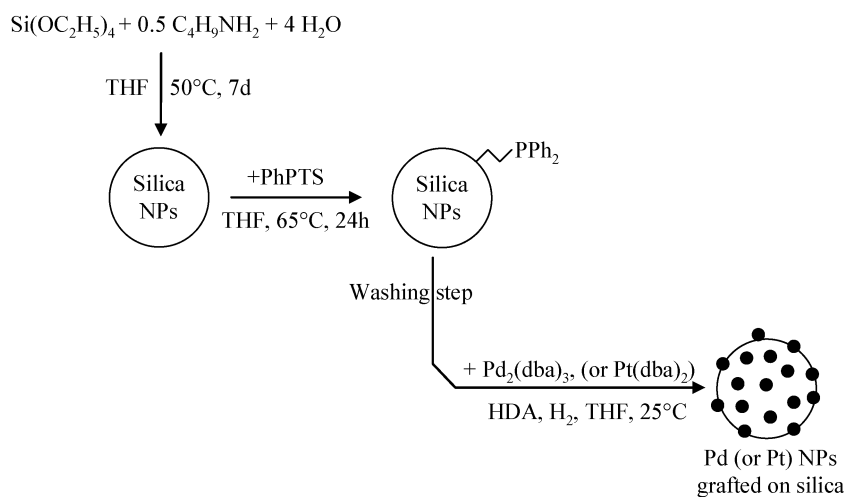


Fig. 4 HRTEM image of Pt NPs immobilised onto silica NPs which have been functionalized with APTES/PTES 1/3 and its FFT pattern (inset).

(PhPETES), following the same procedure as that used for APTES grafting. In contrast to the case of the amino ligand, the use of a co-ligand is not necessary as PhPETES grafting does not induce any aggregation between silica particles, but an

intermediate washing step is here required prior to the addition of the metallic precursor. Indeed, when free PhPETES ligands remain in solution, no metallic NPs are observed, presumably due to side-reactions at the molecular scale, leading to more stable Pt or Pd complexes. The protocol is presented in Scheme 2. In a first step, the PhPETES ligand is directly added to the silica suspension, which is then washed and isolated. Then, HDA, Pd (or Pt) precursor and PhPETES-silica NPs are mixed into THF and pressurised under 3 bar of dihydrogen to form the metallic NPs.

Fig. 5 shows Pd NPs with a mean diameter of 5.1 (0.9) nm, homogeneously immobilised onto the silica surface with a Pd loading of 4.47 wt% determined by ICP-MS (61.5% immobilised Pd yield). The increase in the introduced amount of Pd precursor (which is doubled) allows the Pd content to be increased to 5.95 wt% (the yield of immobilised Pd is about 55%). However, in that case, we observe a clear broadening of the size distribution, the mean diameter of Pd NPs is *ca.* 6.0 (2.3) nm (Fig. 5). The HRTEM image together with the FFT pattern revealed lattice fringes separated by distances of 0.225 nm and 0.194 nm, corresponding, respectively, to the (111) and (200) lattice spacings of the fcc palladium (Fig. 6).



Scheme 2 Synthesis of Pd NPs immobilized on phosphino-functionalized silica NPs.

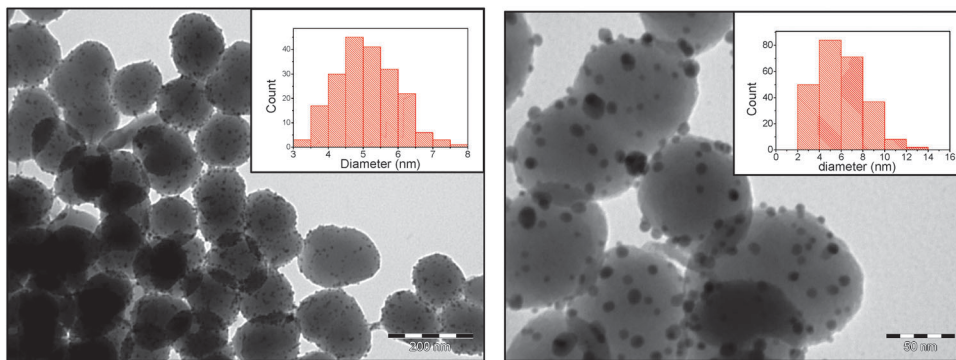


Fig. 5 TEM images of Pd NPs immobilised onto silica particles functionalized with PhPETES (left) and with a double amount of Pd (right) with inserted size distributions.

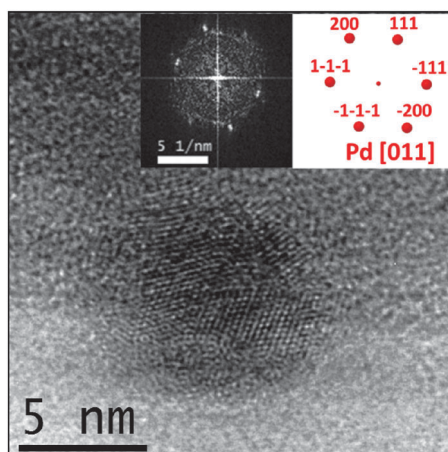


Fig. 6 HRTEM image of Pd NPs immobilised onto silica NPs functionalized with PhPETES and its FFT pattern (inset).

Similarly, formation of Pt NPs was successfully obtained. ICP-MS shows that 56% of the introduced Pt is immobilised onto silica, forming very homogeneously dispersed NPs with a mean diameter of *ca.* 3.1 (0.7) nm (Fig. 7) with a Pt content of 4.57 wt%. The HRTEM image together with the FFT pattern revealed lattice fringes separated by distances of 0.226 nm and

0.196 nm corresponding, respectively, to the (111) and (200) lattice spacings of the fcc platinum (Fig. 7).

According to MAS-NMR experiments, in contrast to PTES and APTES, the grafting of PhPETES appears to be much less efficient. The $^{29}\text{Si}\{\text{H}\}$ spectrum of PhPETES grafted NPs (Fig. S3, ESI[†]) clearly shows the presence of Q₂, Q₃ and Q₄, but T substructure silicon atoms could only be detected as a very minor species (~1%). However, the Cross-Polarization (CP) sequence (Fig. S4, ESI[†]), thanks to the enhancement of surface-localized spins, allows the confirmation of the chemical functionalization and the location at the surface. Consistently, the $^{31}\text{P}\{\text{H}\}$ NMR spectrum (Fig. 8) of the grafted silica NPs displays two main signals at δ –9 and 37 ppm assigned, respectively, to PhPETES grafted on silica NPs (32%) and its corresponding phosphine oxide (64%).³² The oxidation results from the reaction of the phosphine with the silanol groups of the silica NP surface as already evidenced by Bemi *et al.*³³ Last, a weak signal (4%) at δ 27 may arise from hydrogen bonds between phosphine oxide and surface silanol groups.³² In the presence of Pd NPs (Fig. 9), the coordination of the NPs results in the shift of resonance of the phosphine moiety to a chemical shift of around δ 25.⁸ Interestingly, only a very minor amount (~3%) of PhPETES grafted remains uncomplexed. This could explain why it is not possible here to increase the Pd content

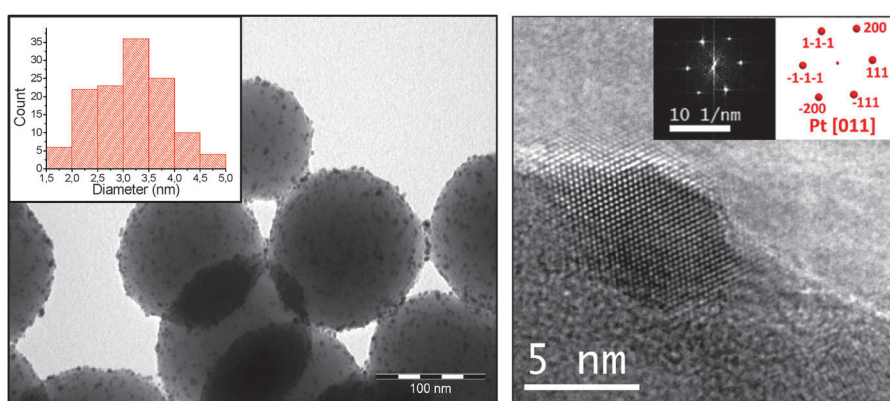


Fig. 7 TEM image of Pt NPs immobilised onto silica NPs functionalized with PhPETES (left with inserted size distribution) and HRTEM image (right with FFT pattern).

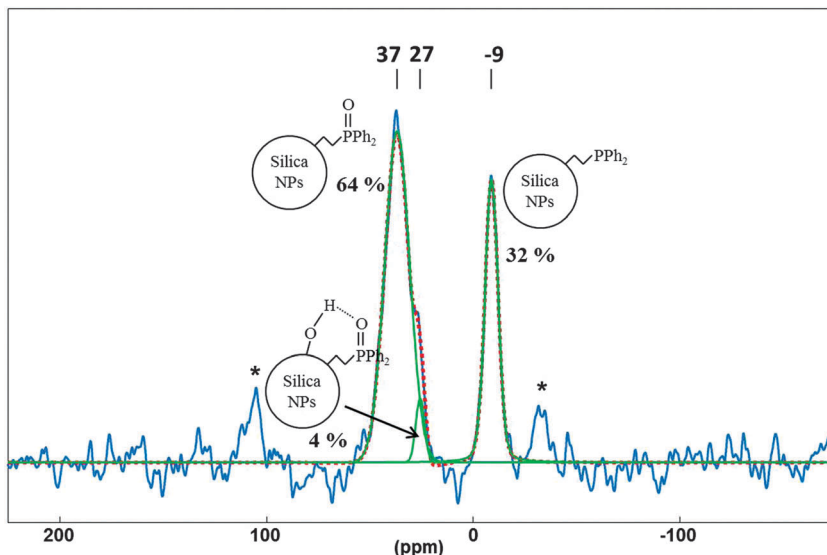


Fig. 8 $^{31}\text{P}\{^1\text{H}\}$ MAS NMR spectrum of silica NPs functionalized with PhPETES. The spectrum was fully deconvoluted using the dmfit software.

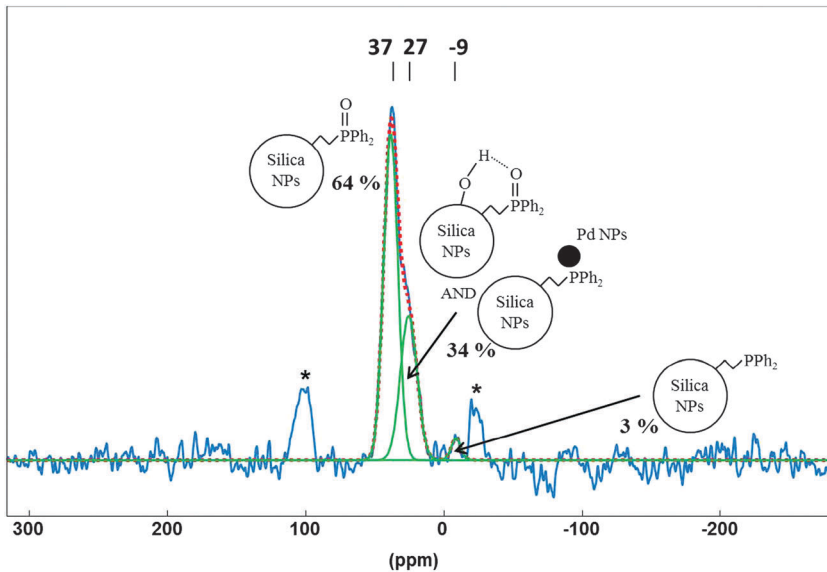


Fig. 9 $^{31}\text{P}\{^1\text{H}\}$ MAS NMR spectrum of Pd NPs immobilised onto silica NPs functionalized with PhPETES. The spectrum was fully deconvoluted using the dmfit software.

without increasing the mean diameter of the Pd NPs. There are not enough phosphino-sites at the surface to allow the formation of more NPs, and hence their growth is favoured.

Table 1 summarizes the characteristics of the different strawberry-like nanomaterials prepared in this article. Catalyst **1** and catalyst **2** refer to the nanomaterials further investigated in catalytic applications (*vide infra*).

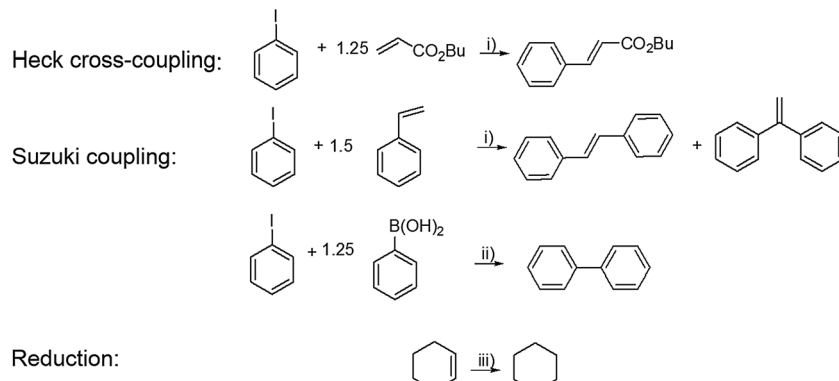
Catalytic tests of Pd-based strawberry-like nano-objects

Pd is a highly effective catalyst in the hydrogenation-dehydrogenation reactions as well as in C–C coupling reactions.^{3,6} In order to evaluate the potentialities of our $\text{SiO}_2@\text{Pd}$ nanomaterials, preliminary catalytic tests were run for different reactions:

Table 1 Characteristics of the prepared nanomaterials (mean diameter of Pd (or Pt) NPs and metal loading)

Ligand	APTES/PTES 1/3		PhPETES	
Metal	Pd	Pt	Pd	Pt
Catalyst 1 Catalyst 2				
NPs diameter (nm)	3.6 (0.8)	1.5 (0.3)	5.1 (0.9)	6.0 (2.3)
Metal loading (wt%)	2.94–6.91	2.14	4.47	5.95
				4.57

the Heck cross-coupling reaction of iodobenzene with butyl acrylate and styrene, Suzuki coupling of phenylboronic acid and iodobenzene and finally, the reduction of cyclohexene by dihydrogen (Scheme 3).



Scheme 3 Evaluation of the catalytic activity of catalysts **1** and **2**. Reagents and conditions: (i) 0.1 mol% Pd, Et₃N (1.5 eq.), DMF, 100 °C. (ii) 0.1 mol% Pd, K₂CO₃ (1.5 eq.), DMF/H₂O (10 : 1), 100 °C. (iii) 0.02 mol% Pd, H₂, 3.5 bar, 75 °C.

The catalytic performance of **1** was first tested in the cross-coupling reaction of butyl acrylate and iodobenzene at 0.1% mol Pd loading using mild conditions (Et₃N, DMF, 100 °C).³⁴ Quantitative conversion was obtained within the first two hours of reaction with 100% selectivity towards butyl cinnamate (Table 2, entry 1). After catalyst separation, mother liquors of the reaction were analysed and only 3.6 ppm of Pd could be detected. Similarly, the catalytic activity of **1** and **2** was evaluated in the coupling of styrene and iodobenzene obtaining high conversion values within the first 4–5 h (76% and 71% for **1** and **2**, respectively, entries 2 and 3) with moderate to high selectivities towards *trans*-stilbene (*ca.* 91%) against 1,1-diphenylethene (*ca.* 9%) and almost quantitative conversion when the reaction mixture was left overnight. **1** and **2** appeared to be also active in the Suzuki coupling of phenylboronic acid and iodobenzene that proceeded smoothly affording 96% yield of biphenyl after 3.5 h in DMF–H₂O at 100 °C (entries 4 and 5). Finally, a preliminary test was done on the hydrogenation of neat cyclohexene at 0.017 mol% of Pd loading using **2** with quantitative conversion and 100% selectivity towards cyclohexane after 23 h. It is worth mentioning that the reaction could be carried out under relatively low pressure (3.5 bar) of dihydrogen in neat cyclohexene while keeping good dispersion. Considering the wide scope of published reaction conditions, the results of these catalytic tests are broadly

comparable, in terms of efficiency and selectivity, to the literature reports on the activity of Pd (complexes or NPs) supported on silica.^{5,12,35–39}

Among the studies tackling the question of the recovery of the catalyst,^{5,34,36,38,40,41} Wang *et al.* describe a remarkable example with the immobilization of palladium NPs on silica nanospheres encapsulated with silica. This catalyst has been used in five consecutive cycles in the cross coupling of styrene and iodobenzene with only a slight loss in activity after the fourth run.³⁸ The recovery of catalyst **2** was here tested in the Heck reaction between butyl acrylate and iodobenzene. As expected, iodobenzene was quantitatively converted within the first two hours with 100% selectivity towards butyl cinnamate. The catalyst could be easily recovered after centrifugation and washed with dichloromethane in open-air. The catalyst was used during eight runs affording butyl cinnamate as the only reaction product (>95% yield within 3 hours, Fig. 10), without significant loss of activity.

Conclusion

Successful immobilization of metallic nanoparticles on silica has been readily achieved by the decomposition of organometallic precursors onto silica spheres prepared in non-alcoholic media (being thus fully compatible with the organometallic chemistry). A family of different strawberry-like nanomaterials has been synthesized using different functional ligands (APTES or PhPETES) on the silica and different immobilised metallic nanoparticles (Pd or Pt). It is remarkable to mention that, in all the cases, the metallic nanoparticles are crystalline, dense and well-distributed on the surface of silica. They display homogeneous spherical morphologies and their mean diameter can vary, according to the functional ligand on the silica spheres, from 3.6 to 6.0 nm for Pd and from 1.5 to 3.1 nm for Pt nanoparticles. The metal loading is adjustable, at least up to 6.91 wt%, as exemplified with Pd. The use of a mixture of APTES-PTES, to functionalize the silica surface, advantageously prevents agglomeration between the silica particles by avoiding the classical interfering cohydrolysis and polycondensation reactions. It is noteworthy that the ratio of APTES/PTES has to be increased

Table 2 Screening of the catalytic activity of catalysts **1** and **2** in C–C cross-coupling reactions of iodobenzene with different substrates

Entry	Substrate	Catalyst ^a	Time (h)	Yield ^b (%)
1		1	2	98
2		1	3.7	76 (90) ^c
			25	90 (91)
3		2	5.6	71 (91)
			27	95 (92)
4		1	3.4	94
5		2	3.4	96

^a 0.1 mol% of catalyst loading and temperature = 100 °C. ^b 1,3,5-Triphenoxybenzene as the internal standard. ^c Values in parentheses indicate selectivity towards *trans* stilbene.

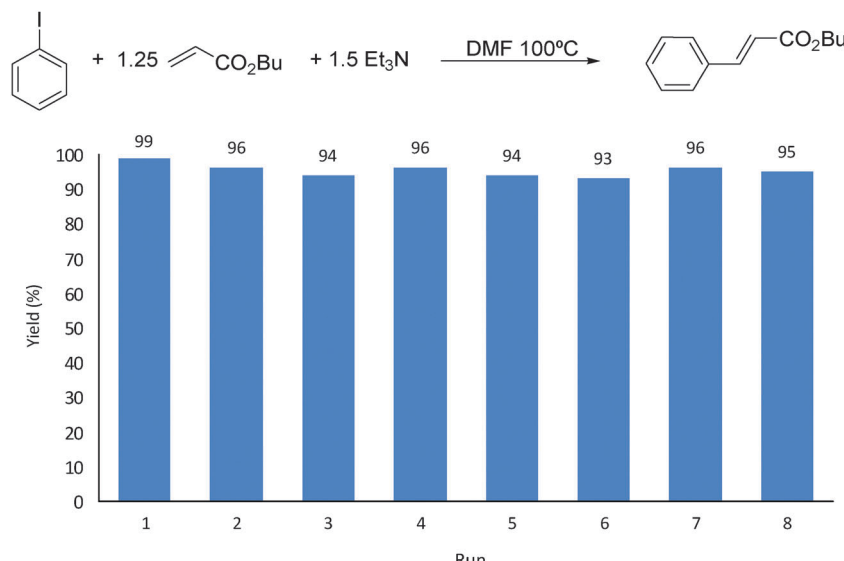


Fig. 10 Recovery test of **2** in the Heck coupling of iodobenzene and butyl acrylate.

from 1/1 to 1/3 to allow the homogeneity of the dispersion of the Pd nanoparticles at the surface. According to preliminary catalytic tests, the nanomaterial constituted by Pd NPs immobilised on the PhPETES-functionalized silica nanomaterial appears as a promising catalyst in C–C cross-coupling reactions.

The synthetic protocol reported in this article is very easy to be implemented (one pot, low temperatures). It can be adapted for different ligands and different metals, providing a wide versatility. The examples (Pd and Pt nanoparticles) which are presented here are far away to be exhaustive. Indeed, the controlled synthesis of different metallic nanoparticles (such as Ru, Rh or Ir)^{24,26,42} has been described, by using the same organometallic method. Thus, we could expect to produce such different metal NPs on the surface of silica spheres, in the same way.

Experimental section

General procedures and materials

All manipulations were carried out under an argon atmosphere using a Fischer–Porter bottle and vacuum line techniques, or in a glovebox. Tetraethoxysilane (TEOS) was purchased from Alfa Aesar, hexadecylamine (HDA; ≥99%) and butylamine (BA; ≥99.5%) from Fluka, aminopropyltriethoxysilane (APTES; ≥98%) and propyltriethoxysilane (PTES; ≥97%) from Aldrich, 2-(diphenylphosphino)ethyltriethoxysilane (PhPETES) from Gelest. Tetrahydrofuran was purchased from SDS (99.9%), dried and distilled over sodium/benzophenone. $\text{Pd}_2(\text{dba})_3$ and $\text{Pt}(\text{dba})_2$ were purchased from NanoMeps. All reagents and solvents were degassed before use by using three freeze–pump–thaw cycles. Samples for TEM analysis were prepared in a glovebox by slow evaporation of a drop of the colloidal solution deposited onto a carbon-covered copper grid. TEM analysis was performed at the “Service Commun de Microscopie Electronique de l’Université Paul Sabatier” (TEMSCAN) on a JEOL JEM 200 CX electron microscope

operating at 200 kV with a point resolution of 4.5 Å and on a JEOL JEM 1011 electron microscope operating at 100 kV with a point resolution of 4.5 Å. The size distributions were determined by measuring *ca.* 150 particles using the Image J software (variation range is given by 3σ). Crystalline structures are attributed on the basis of several HRTEM images together with the FFT patterns revealing the same lattice fringes on different NPs. Solid-state NMR experiments were performed on a Bruker Avance 400WB equipped with a 4 mm probe, the sample rotation frequency being set at 12 kHz unless otherwise indicated. All ^1H , ^{29}Si , and ^{13}C chemical shifts are reported using the δ scale and are referenced to tetramethylsilane (TMS) at 0 ppm. ^{31}P chemical shifts are reported and referenced to an external H_3PO_4 sample. Microanalysis was performed by the “Service de microanalyses du Laboratoire de Chimie de Coordination” (C, H, N) or by Antellis company (Pd, Pt).

Catalytic tests were monitored by GC-FID in an Agilent 6890. TecknoKR TRB-FFAP (25 m, 320 µm, Tecknacroma) was used as the stationary phase and He as a carrier gas at a constant pressure of 16 psi with a split ratio of 15 and an inlet temperature of 230 °C. The FID detector was operated at 250 °C with a hydrogen flow of 40 mL min⁻¹, air flow 450 mL min⁻¹ and an He make-up flow of 45 mL min⁻¹. The oven was operated at an initial temperature of 40 °C for 5 minutes followed by a ramp of 15 °C min⁻¹ to 200 °C and then maintained for 4 minutes. Reactants and products were calibrated using commercially available standards. 1,3,5-Trimethoxybenzene was used as the internal standard. Retention times were as follows: 8.12 min for *N,N*-dimethylformamide, 15.27 min for 1,3,5-trimethoxybenzene, 10.13 min for iodobenzene, 6.83 min for styrene, 5.06 min for butyl acrylate, 16.58 min for *trans*-butylcinnamate, 14.96 min for 1,1-diphenylethene, 18.25 min for *trans*-stilbene, and 14.14 min for biphenyl. Palladium contents in the mother liquors were analyzed by atomic absorption on a Perkin Elmer Atomic Absorption 2100 and a Perkin Elmer Atomic Absorption 3100 using a Pd lamp. Mother liquor samples were concentrated prior to be digested in boiling HCl/HNO_3 3/1.

Palladium contents in the solid catalyst samples were measured by Antellis.

Nanomaterials synthesis

Pd grafting on APTES/PTES 1/1 silica NPs. Tetraethoxysilane (267 μ L, 1.20 mmol) is added to a solution of butylamine (60 μ L, 0.60 mmol) in tetrahydrofuran (10 mL) in a Fischer–Porter bottle at room temperature under vigorous stirring. After 10 min, water (86 μ L, 4.8 mmol) is injected into this mixture which is stirred at 50 °C for seven days. The resulting milky suspension is allowed to cool down and then APTES (84 μ L, 0.36 mmol) and PTES (83 μ L, 0.36 mmol) are added to the mixture that is then stirred at 65 °C. After 24 h, the mixture is again allowed to cool down and HDA (97 mg, 0.40 mmol) and $\text{Pd}_2(\text{dba})_3$ (18.3 mg, 0.02 mmol) are added. The bottle is then pressurized under 3 bar of dihydrogen and the resulting solution stirred for 24 h at room temperature. The dihydrogen is then vented and the resulting black suspension is centrifuged at 5000 rpm for 15 min, yielding a black solid at the bottom of the tubes. The supernatant is eliminated and the precipitate is then washed three times with tetrahydrofuran. A black powder is obtained after drying the precipitate under vacuum for 6 h. Elemental analysis: C, 13.87; H, 2.42; N, 2.71; Pd, 2.98%.

Pd grafting on APTES/PTES 1/3 silica NPs. Tetraethoxysilane (536 μ L, 2.40 mmol) is added to a solution of butylamine (119 μ L, 1.20 mmol) in tetrahydrofuran (20 mL) in a Fischer–Porter bottle at room temperature under vigorous stirring. After 10 min, water (173 μ L, 9.6 mmol) is injected into this mixture which is stirred at 50 °C for seven days. The resulting milky suspension is allowed to cool down and then APTES (84 μ L, 0.36 mmol) and PTES (250 μ L, 1.08 mmol) are added to the mixture that is then stirred at 65 °C. After 24 h, the mixture is again allowed to cool down and HDA (194 mg, 0.80 mmol) and $\text{Pd}_2(\text{dba})_3$ (36.6 mg, 0.04 mmol) are added. The bottle is then pressurized under 3 bar of dihydrogen and the resulting solution stirred for 24 h at room temperature. The dihydrogen is then vented and the resulting black suspension is centrifuged at 5000 rpm for 15 min, yielding a black solid at the bottom of the tubes. The supernatant is eliminated and the precipitate is then washed three times with tetrahydrofuran. A black powder is obtained after drying the precipitate under vacuum for 6 h. Elemental analysis: C, 11.61; H, 2.66; N, 1.76; Pd, 2.94%.

Pd grafting on APTES/PTES 1/3 silica NPs doubling the amount of Pd. Tetraethoxysilane (536 μ L, 2.40 mmol) is added to a solution of butylamine (119 μ L, 1.20 mmol) in tetrahydrofuran (20 mL) in a Fischer–Porter bottle at room temperature under vigorous stirring. After 10 min, water (173 μ L, 9.6 mmol) is injected into this mixture which is stirred at 50 °C for seven days. The resulting milky suspension is allowed to cool down and then APTES (84 μ L, 0.36 mmol) and PTES (250 μ L, 1.08 mmol) are added to the mixture that is then stirred at 65 °C. After 24 h, the mixture is again allowed to cool down and HDA (388 mg, 1.60 mmol) and $\text{Pd}_2(\text{dba})_3$ (73 mg, 0.08 mmol) are added. The bottle is then pressurized under 3 bar of dihydrogen and the resulting solution stirred for 24 h at room temperature. The dihydrogen is then vented and the resulting black suspension

is centrifuged at 5000 rpm for 15 min, yielding a black solid at the bottom of the tubes. The supernatant is eliminated and the precipitate is then washed three times with tetrahydrofuran. A black powder is obtained after drying the precipitate under vacuum for 6 h. Elemental analysis Pd, 6.90%.

Pt grafting on APTES/PTES 1/3 silica NPs. Tetraethoxysilane (536 μ L, 2.40 mmol) is added to a solution of butylamine (119 μ L, 1.20 mmol) in tetrahydrofuran (20 mL) in a Fischer–Porter bottle at room temperature under vigorous stirring. After 10 min, water (173 μ L, 9.6 mmol) is injected into this mixture which is stirred at 50 °C for seven days. The resulting milky suspension is allowed to cool down and then APTES (84 μ L, 0.36 mmol) and PTES (250 μ L, 1.08 mmol) are added to the mixture that is then stirred at 65 °C. After 24 h, the mixture is again allowed to cool down and HDA (194 mg, 0.80 mmol) and $\text{Pt}(\text{dba})_2$ (26.5 mg, 0.04 mmol) are added. The bottle is then pressurized under 3 bar of dihydrogen and the resulting solution stirred for 24 h at room temperature. The dihydrogen is then vented and the resulting black suspension is centrifuged at 5000 rpm for 15 min, yielding a black solid at the bottom of the tubes. The supernatant is eliminated and the precipitate is then washed three times with tetrahydrofuran. A black powder is obtained after drying the precipitate under vacuum for 6 h. Elemental analysis: C, 8.52; H, 2.08; N, 1.88%; Pt, 2.14%.

Pd grafting on PhPETES silica NPs. Tetraethoxysilane (267 μ L, 1.20 mmol) is added to a solution of butylamine (61 μ L, 0.60 mmol) in tetrahydrofuran (10 mL) in a Fischer–Porter bottle at room temperature under vigorous stirring. After 10 min, water (86 μ L, 4.8 mmol) is injected into this mixture which is stirred at 50 °C for seven days. The resulting milky suspension is allowed to cool down and then PhPETES (258 μ L, 0.72 mmol) is added to the mixture that is then stirred at 65 °C. After 24 h, the mixture is again allowed to cool down and then the resulting milky suspension is centrifuged at 20 000 rpm for 20 min, yielding particles as a white solid at the bottom of the tubes. The supernatant is eliminated and the precipitate is then washed three times with tetrahydrofuran. A last addition of tetrahydrofuran (10 mL) allows again the dispersion the NPs and then HDA (96.8 mg, 0.40 mmol) and $\text{Pd}_2(\text{dba})_3$ (18.3 mg, 0.02 mmol) are added. The bottle is then pressurized under 3 bar of dihydrogen and the resulting solution stirred for 24 h at room temperature. The dihydrogen is then vented and the resulting black suspension is centrifuged at 5000 rpm for 15 min, yielding a black solid at the bottom of the tubes. The supernatant is eliminated and the precipitate is then washed three times with tetrahydrofuran. A black powder is obtained after drying the precipitate under vacuum for 6 h. Elemental analysis: Pd, 4.11%.

Pd grafting on PhPETES silica NPs doubling the amount of Pd. Tetraethoxysilane (267 μ L, 1.20 mmol) is added to a solution of butylamine (61 μ L, 0.60 mmol) in tetrahydrofuran (10 mL) in a Fischer–Porter bottle at room temperature under vigorous stirring. After 10 min, water (86 μ L, 4.8 mmol) is injected into this mixture which is stirred at 50 °C for seven days. The resulting milky suspension is allowed to cool down and then PhPETES (258 μ L, 0.72 mmol) is added to the mixture that is then stirred at 65 °C. After 24 h, the mixture is again allowed to cool down and then

the resulting milky suspension is centrifuged at 20 000 rpm for 20 min, yielding particles as a white solid at the bottom of the tubes. The supernatant is eliminated and the precipitate is then washed three times with tetrahydrofuran. A last addition of tetrahydrofuran (10 mL) allows again the dispersion the NPs and then HDA (194 mg, 0.80 mmol) and Pd₂(dba)₃ (36.6 mg, 0.04 mmol) are added. The bottle is then pressurized under 3 bar of dihydrogen and the resulting solution stirred for 24 h at room temperature. The dihydrogen is then vented and the resulting black suspension is centrifuged at 5000 rpm for 15 min, yielding a black solid at the bottom of the tubes. The supernatant is eliminated and the precipitate is then washed three times with tetrahydrofuran. A black powder is obtained after drying the precipitate under vacuum for 6 h. Elemental analysis: Pd, 5.95%.

Pt grafting on PhPETES silica NPs. Tetraethoxysilane (267 µL, 1.20 mmol) is added to a solution of butylamine (61 µL, 0.60 mmol) in tetrahydrofuran (10 mL) in a Fischer–Porter bottle at room temperature under vigorous stirring. After 10 min, water (86 µL, 4.8 mmol) is injected into this mixture which is stirred at 50 °C for seven days. The resulting milky suspension is then allowed to cool down and then PhPETES (258 µL, 0.72 mmol) is added to the mixture that is then stirred at 65 °C. After 24 h, the mixture is again allowed to cool down and then the resulting milky suspension is centrifuged at 20 000 rpm for 20 min, yielding particles as a white solid at the bottom of the tubes. The supernatant is eliminated and the precipitate is then washed three times with tetrahydrofuran. A last addition of tetrahydrofuran (10 mL) allows again the dispersion the NPs and then HDA (194 mg, 0.80 mmol) and Pt(dba)₂ (26.5 mg, 0.02 mmol) are added. The bottle is then pressurized under 3 bar of dihydrogen and the resulting solution stirred for 24 h at room temperature. The dihydrogen is then vented and the resulting black suspension is centrifuged at 5000 rpm for 15 min, yielding a black solid at the bottom of the tubes. The supernatant is eliminated and the precipitate is then washed three times with tetrahydrofuran. A black powder is obtained after drying the precipitate under vacuum for 6 h. Elemental analysis: Pd, 4.57%.

Catalytic tests

Hydrogenation of cyclohexene using catalyst 2. In a Fischer–Porter bottle, 2 (3.0 mg, 1.68 × 10⁻³ mmol Pd) was dispersed in cyclohexene (990 µL, 9.8 mmol). The system was pressurized with dihydrogen (3.5 bar) for 3 minutes, sealed and then stirred at 75 °C for 23 h. The bottle was then allowed to cool and the crude mixture was analyzed by ¹H NMR observing the sole presence of cyclohexane. ¹H NMR (400 MHz, CDCl₃): 1.33 (s, 12H). ¹³C{¹H} NMR (100 MHz, CDCl₃): 26.96 (Fig. S5, ESI†).

Cross-coupling reaction of butyl acrylate and iodobenzene using catalyst 1. In a conditioned Schlenk, 1 (4.6 mg, 1.38 × 10⁻³ mmol Pd), anhydrous DMF (2.0 mL), a known amount of 1,3,5-trimethoxybenzene, iodobenzene (168 µL, 1.5 mmol), butyl acrylate (270 µL, 1.87 mmol) and triethylamine (311 µL, 2.25 mmol) are added. The resulting solution is stirred at 100 °C and the progress of the reaction monitored by GC.

Cross-coupling reaction of styrene and iodobenzene using catalyst 2. In a conditioned Schlenk, 2 (5.0 mg, 2.80 × 10⁻³ mmol Pd), anhydrous DMF (2.5 mL), a known amount of 1,3,5-trimethoxybenzene, iodobenzene (313 µL, 2.8 mmol), styrene (480 µL, 4.2 mmol) and triethylamine (581 µL, 4.2 mmol) are added. The resulting solution is stirred at 100 °C and the progress of the reaction monitored by GC.

Cross-coupling reaction of styrene and iodobenzene using catalyst 1. In a conditioned Schlenk, 1 (5.0 mg, 1.50 × 10⁻³ mmol Pd), anhydrous DMF (2.0 mL), a known amount of 1,3,5-trimethoxybenzene, iodobenzene (168 µL, 1.5 mmol), styrene (257 µL, 2.25 mmol) and triethylamine (311 µL, 2.25 mmol) are added. The resulting solution is stirred at 100 °C and the progress of the reaction monitored by GC.

Cross-coupling reaction of phenylboronic acid and iodobenzene using catalyst 2. In a conditioned Schlenk, 2 (5.0 mg, 2.80 × 10⁻³ mmol Pd), anhydrous DMF (4.5 mL), a known amount of 1,3,5-trimethoxybenzene, iodobenzene (313 µL, 2.8 mmol), phenylboronic acid (511 mg, 4.2 mmol), potassium carbonate (580 mg, 4.2 mmol) and water (0.45 mL) are added. The resulting solution is stirred at 100 °C and the progress of the reaction monitored by GC.

Cross-coupling reaction of phenylboronic acid and iodobenzene using catalyst 1. In a conditioned Schlenk, 1 (3.8 mg, 1.14 × 10⁻³ mmol Pd), anhydrous DMF (2.5 mL), a known amount of 1,3,5-trimethoxybenzene, iodobenzene (128 µL, 1.14 mmol), phenylboronic acid (208 mg, 1.71 mmol), potassium carbonate (236 mg, 1.71 mmol) and water (0.25 mL) are added. The resulting solution is stirred at 100 °C and the progress of the reaction monitored by GC.

Acknowledgements

A.C. is indebted to the Spanish Ministerio de Ciencia y Tecnología for a Post-Doctoral grant I. S. is indebted to the “Departamento de Industria de la Comunidad Foral de Navarra” for a grant. We thank Cécile Garcia Marcelot for helpful treatment of HRTEM images.

References

- B. J. Jankiewicz, D. Jamiola, J. Choma and M. Jaroniec, *Adv. Colloid Interface Sci.*, 2012, **170**, 28–47.
- D. Astruc, F. Lu and J. Ruiz Aranzaes, *Angew. Chem., Int. Ed.*, 2005, **44**, 7852–7872.
- N. Yan, C. Xiao and Y. Kou, *Coord. Chem. Rev.*, 2010, **254**, 1179–1218.
- Chiral Catalyst Immobilization and Recycling*, ed. D. E. D. Vos, I. F. J. Vankelecom and P. A. Jacobs, Wiley-VCH, 2000.
- S. Shylesh, L. Wang and W. R. Thiel, *Adv. Synth. Catal.*, 2010, **352**, 425–432.
- A. Roucoux, J. Schulz and H. Patin, *Chem. Rev.*, 2002, **102**, 3757–3778.
- N. J. S. Costa and L. M. Rossi, *Nanoscale*, 2012, **4**, 5826–5834.
- V. Polshettiwar, C. Len and A. Fihri, *Coord. Chem. Rev.*, 2009, **293**, 2599–2626.

- 9 N. J. S. Costa, P. K. Kiyohara, A. L. Monteiro, Y. Coppel, K. Philippot and L. M. Rossi, *J. Catal.*, 2010, **276**, 382–389.
- 10 M. J. Jacinto, O. H. C. F. Santos, R. F. Jardim, R. Landers and L. M. Rossi, *Appl. Catal., A*, 2009, **360**, 177–182.
- 11 A. Peled, M. Naddaka and J.-P. Lellouche, *J. Mater. Chem.*, 2012, **22**, 7580–7583.
- 12 L. M. Rossi, I. M. Nangoi and N. J. S. Costa, *Inorg. Chem.*, 2009, **48**, 4640–4642.
- 13 J. Y. Shin, B. S. Lee, Y. Jung, S. J. Kim and S.-G. Lee, *Chem. Commun.*, 2007, 5238–5240.
- 14 M. J. Jacinto, O. H. C. F. Santos, R. Landers, P. K. Kiyohara and L. M. Rossi, *Appl. Catal., B*, 2009, **90**, 688–692.
- 15 M. J. Jacinto, P. K. Kiyohara, S. H. Masunaga, R. F. Jardim and L. M. Rossi, *Appl. Catal., A*, 2008, **338**, 52–57.
- 16 S. L. Westcott, S. J. Oldenburg, T. R. Lee and N. J. Halas, *Langmuir*, 1998, **14**, 5396–5401.
- 17 K. Gude and R. Narayanan, *J. Phys. Chem. C*, 2010, **114**, 6356–6362.
- 18 S.-K. Lee, X. Liu, V. S. Cabeza and K. F. Jensen, *Lab Chip*, 2012, **12**, 4080–4084.
- 19 M. Guerrero, N. J. S. Costa, L. L. R. Vono, L. M. Rossi, E. V. Gusevskaya and K. Philippot, *J. Mater. Chem. A*, 2013, **1**, 1441–1449.
- 20 N. El Hawi, C. Nayral, F. Delpech, Y. Coppel, A. Cornejo, A. Castel and B. Chaudret, *Langmuir*, 2009, **25**(13), 7540–7546.
- 21 B. Chaudret and K. Philippot, *Oil Gas Sci. Technol.*, 2007, **62**(6), 799–817.
- 22 C. Amiens and B. Chaudret, *Mod. Phys. Lett. B*, 2007, **21**(18), 1133–1141.
- 23 L.-M. Lacroix, S. Lachaize, J. Carrey, M. Respaud and B. Chaudret, *Actual. Chim.*, 2011, **351**, 28–35.
- 24 P. Lara, K. Philippot and B. Chaudret, *ChemCatChem*, 2013, **5**, 28–45.
- 25 I. Favier, M. Gomez, G. Muller, M. R. Axet, S. Castillon, C. Claver, S. Jansat, B. Chaudret and K. Philippot, *Adv. Synth. Catal.*, 2007, **349**, 2459–2469.
- 26 P.-J. Debouttière, Y. Coppel, A. Denicourt-Nowicki, A. Roucoux, B. Chaudret and K. Philippot, *Eur. J. Inorg. Chem.*, 2012, 1229–1236.
- 27 N. Gartmann and D. Brühwiler, *Chimia*, 2011, **65**(4), 250–252.
- 28 M. Tristany, K. Philippot, Y. Guari, V. Collière, P. Lecante and B. Chaudret, *J. Mater. Chem.*, 2010, **20**, 9523–9530.
- 29 R. Mouawia, A. Mehdi, C. Reyé and R. J. P. Corriu, *J. Mater. Chem.*, 2008, **18**, 4193–4203.
- 30 E. Ramirez, S. Jansat, K. Philippot, P. Lecante, M. Gomez, A. M. Masdeu-Bulto and B. Chaudret, *J. Organomet. Chem.*, 2004, **689**, 4601–4610.
- 31 A. Rodriguez, C. Amiens, B. Chaudret, M.-J. Casanove, P. Lecante and J. S. Bradley, *Chem. Mater.*, 1996, **8**, 1978–1986.
- 32 R. A. Komoroski, A. J. Majistro and P. A. Nicholas, *Inorg. Chem.*, 1986, **25**, 3917–3925.
- 33 L. Bemi, H. C. Clark, J. A. Davies, C. A. Fyfe and R. E. Wasylishen, *J. Am. Chem. Soc.*, 1982, **104**, 438–445.
- 34 S. Jana, B. Dutta, R. Bera and S. Koner, *Inorg. Chem.*, 2008, **47**, 5512–5520.
- 35 A. Fihri, D. Cha, M. Bouhrara, N. Almana and V. Polshettiwar, *ChemSusChem*, 2012, **5**, 85–89.
- 36 Z. Chen, Z.-M. Cui, F. Niu, L. Jiang and W.-G. Song, *Chem. Commun.*, 2010, **46**, 6524–6526.
- 37 A. V. Biradar, A. A. Biradar and T. Asefa, *Langmuir*, 2011, **27**, 14408–14418.
- 38 Y. Wang, A. V. Biradar, C. T. Duncan and T. Asefa, *J. Mater. Chem.*, 2010, **20**, 7834–7841.
- 39 B. Blanco, M. Brissart, M. Moreni-Manas, R. Pleixats, A. Mehdi, C. Reyé, S. Bouquillon, F. Hénin and J. Muzart, *Appl. Catal., A*, 2006, **297**, 117–124.
- 40 G. Martra, L. Bertinetti, C. Gerbaldi, R. Maggi, G. Sartori and S. Coluccia, *Catal. Lett.*, 2009, **132**, 50–57.
- 41 P. Wang, Q. Lu and J. Li, *Catal. Lett.*, 2009, **131**, 444–450.
- 42 A. Gual, C. Godard, K. Philippot, B. Chaudret, A. Denicourt-Nowicki, A. Roucoux, S. Castillon and C. Claver, *ChemSusChem*, 2009, **2**(8), 769–779.